Science World Journal Vol. 20(No 1) 2025 https://dx.doi.org/10.4314/swj.v20i1.16
www.scienceworldjournal.org
ISSN: 1597-6343 (Online), ISSN: 2756-391X (Print)
Published by Faculty of Science, Kaduna State University

Full Length Research Article

EVALUATION OF GEOTHERMAL ENERGY RESOURCE POTENTIAL IN NORTHEASTERN NIGERIA USING SPECTRAL ANALYSIS OF AEROMAGNETIC DATA

*[1,2]Usman Ahmed Kehinde; [1]Osumeje Joseph; [3]Bello Yusuf Ayoola; [1]Hassan Yusuf Adigun; [1]Onuh Echeche

[1]Department of Physics, Faculty of Physical Sciences, Ahmadu Bello University, Zaria, Nigeria
[2]Department of Applied and Environmental Geophysics, Faculty of Natural Sciences, Comenius University, Bratislava, Slovakia
[3]The Air Force Institute of Technology (AFIT), Kaduna, Nigeria

*Corresponding Author Email Address:ahmedkehindeusman@gmail.com, akusman@abu.edu.ng Phone: +234 8164594389

ABSTRACT
Nigeria, despite its continued population growth, does not generate enough power for the country's overall usage. The need for renewable and alternative sources of energy necessitates the need for this research work. The spectral analysis of aeromagnetic data was carried out with the purpose of evaluating geothermal energy resource potential in northeastern Nigeria. The study area is bounded by latitudes 9°30′00′′ N – 14°0′00′′ N and longitudes 9°0′00′′ E – 14°30′00′′ E. Separation of regional and residual was carried out on the total magnetic field intensity (TMI) using the fitting method of order one. For the spectral analysis, a radial power spectrum was applied to the residual data, which was divided into eighty-five (85) square blocks (each block representing each sheet), and each block was analyzed by plotting the log of the power spectrum against the wavenumber to obtain depths to the top (Z_t) and centroid (Z_o) of the magnetic anomalous body (source). These depths were used to evaluate the Curie-point depth (CPD), geothermal gradient (GTG), and near-surface heat flow (HF) in the study area. The results revealed that the values of curie point depth (Z_b) range from 10.28 km to 50.61 km with a mean of 34.02 km, geothermal gradient values range from 11.45 °Ckm^{-1} to 56.41 °Ckm^{-1} with a mean of 18.14 °Ckm^{-1} and heat flow values range from 28.65 mWm^{-2}) to 141.03 m mWm^{-2} with a mean value of 45.36 mWm^{-2}. The heat flow has its maximum values around the southwestern portion of the study area. This portion and the entire study area with low values of CPD and high values of heat flow might probably be good geothermal sources and thereby further recommended for detailed geothermal exploration.

Keywords: Aeromagnetic Data, Geothermal, Curie Point Depth, Geothermal Gradient, Heat Flow

INTRODUCTION

The need for development can be achieved through the availability of sufficient energy or energy source (Cole, 2014). Energy can also be generated from earth's subsurface in form of geothermal (Lawal *et al*., 2018). Geothermal energy is a clean energy source (Sunday, 2015) and has been exploited by several developed countries like United States of America, Indonesia, Philippines, Turkey, New Zealand etc.

Nigeria does not generate enough energy for the country's overall consumption despite the country's continued population growth and the need for more power for both residential and industrial use. Although geothermal energy has been gradually incorporated into some African and global countries, Nigeria cannot be completely excluded from the possibility of investigating geothermal energy (Ewa and Kryrowska, 2010). There has ever been a more pressing need to investigate the generation of electric power from other sources to complement the ones being used. According to Lawal *et al.* (2018), geothermal energy is the utilization of heat energy within the earth, whereby the earth's heat engine is powered by the cooling of the crust and the heating of the lower crust and mantle by thermal decay of radioactive isotopes. As a result, the temperature rises with depth below the surface. Because energy is essential for socioeconomic development and the eradication of poverty, access to clean energy services is a significant challenge facing the African continent (Oyedepo, 2012). It has been reported by many researchers that geothermal energy is a clean and sustainable energy source, contained in intense heat, that continually flows outward from deep within the earth's core (Hulen and Wright, 2001; Nemzer *et al.,* 2004; Nemzer *et al.,* 2009; Obande *et al.,* 2014; Sunday, 2015). It utilizes the earth's natural heat by sourcing superheated water found in joints and fractures in the earth's crust (Abraham, 2011). According to Nemzer *et al.* (2009), GEA (2012), and GRC (2017), the geothermal energy resource is greater than the combined resources for coal, petroleum, natural gas and Uranium. Geothermal energy is useful in heat pumps, geothermal direct heating, and power generation (Bowyer et al., 2011; Renewable Energy World, 2019).

The thermal energy extracted for geothermal power generation represents only a negligible fraction of the Earth's total heat content; thus, geothermal energy is generally classified as renewable and sustainable (Fridleifsson *et al*., 2008). Furthermore, geothermal energy is seen to offer significant potential for mitigating global warming due to its minimal emissions (Turcotte and Schubert, 2002). According to the World Energy Council website, Nigeria produces 4.39 megatons of gas and 120 million tons of oil annually (World Energy Council, 2014). It is therefore necessary to counter the effects of greenhouse gases produced in the country, which are dangerously high due to the high production of million/mega tons of oil and gas and the high consumption of these because of insufficient electricity supply. Since the technology and equipment used in the production of geothermal energy are quite like those used in the oil and gas industries, the idea of using renewable energy should be strongly supported throughout the nation. Therefore, developing its geothermal resources will be extremely advantageous for Nigeria, an oil-rich region (Cole, 2014).

In this investigation, the depth to the bottom of magnetic sources was estimated using spectral analysis, often known as the centroid approach. The centroid approach is one of the most often utilized

Science World Journal Vol. 20(No 1) 2025 https://dx.doi.org/10.4314/swj.v20i1.16
www.scienceworldjournal.org
ISSN: 1597-6343 (Online), ISSN: 2756-391X (Print)
Published by Faculty of Science, Kaduna State University

techniques because, in comparison to other methods, it provides better estimates with fewer depth mistakes (Ravat et al., 2007). The technique of determining and analyzing the potential field data's spectrum is known as spectral analysis. Based on the idea that a magnetic field measured at the surface can be regarded as an integral of a magnetic signature from any depth, the spectral depth approach was developed (Rabeh et al., 2008). To assess the potential for geothermal energy resources in northeastern Nigeria, this study entails a quantitative estimate of subsurface heat flow (HF) anomalies, geothermal gradients (GTG), and Curie-point depths (CPD). Numerous studies have revealed that magnetic data can be widely applied to ascertain the thermal structure of the crust of the earth in a variety of geologic settings (Mohammed et al., 2019).

Description of Study Area and Geothermal Implications

The study area (Figures 1a&b) is bounded by latitudes 9˚30′00′′ N – 14˚0′00′′ N and longitudes 9˚0′00′′ E – 14˚30′00′′ E and comprises Adamawa, Bauchi, Borno, Gombe, Taraba, and Yobe states and part of north central states in the northern part of Nigeria. The area comprises three major groups of rocks, namely the Precambrian Basement Complex, Cretaceous Sediments, and Tertiary/Quaternary volcanic rocks of the Biu Plateau (Jalo, 2015). In the late 1980s through 1990s, the Basement Complex of northeastern Nigeria and, to some extent, the Cretaceous sediment in the region were studied concerning the favorability, structural settings, and geochemistry of uranium (U) mineralization (Funtua et al., 1999; Jalo, 2015). Numerous low-grade uranium mineralizations occur within the Gubrunde horst (basement complex) and in the sedimentary rocks adjacent to the Peta syncline. Other U mineralization include those of Ghumchi and Mika (Dada and Suh, 2006). The mineralization commonly occurs in fractured, sheared or brecciated zones of granites which are sometime in association with later rhyolites. (Islam and Baba, 1990). The presence of hot springs and basins, the Tertiary and Quaternary volcanic rocks, and U mineralization in north-eastern Nigeria are all good geological evidence of potential geothermal energy.

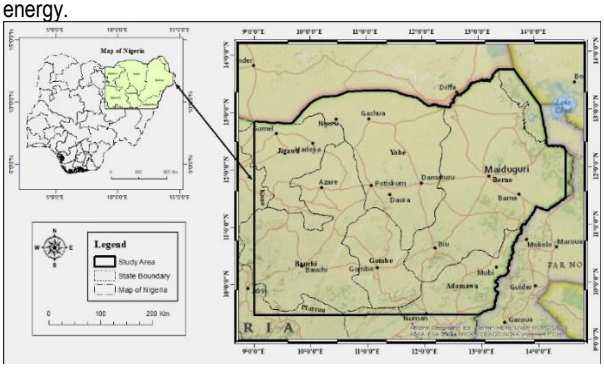

Figure 1(a): Geological map of Nigeria showing the Proposed Study Area (digitized)

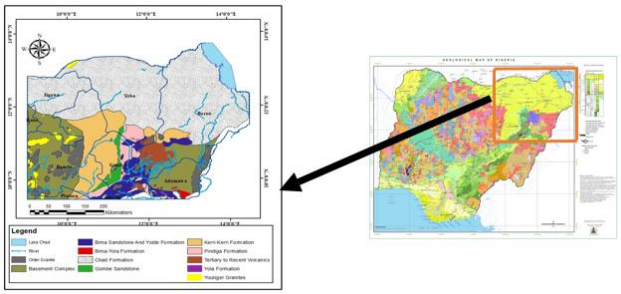

Figure 1(b): Geological Map of the Study Area (Adapted From NGSA, 2011).

MATERIALS AND METHODS

The data used in this study comes from an aeromagnetic survey that Fugro conducted in 2005-2007 on behalf of the Nigeria Geological Survey Agency. The data has a terrain clearance of 80 meters and flight height of about 500 meters above the ground and tie line spacings 2 kilometers, in the NW-SE and NE-SW directions (Sunday *et al.,* 2022). The data acquired by Fugro was so arranged and save such that the X column represent longitude/easting, Y column represent latitude/northing, and the Z column represents the total magnetic intensity. The Total Magnetic Field Intensity value (Z) was stripped of 33,000 nT for ease of processing. Therefore, a simple arithmetic addition of 33,000 nT to each value of Z column was done after the purchase of the data from NGSA to yield the Z Total before any further processing could be deemed valid. The X and Y columns were georeferenced in the Universal Transverse Mercator (UTM) projection system and then set as the preferred columns.

Eighty-five (85) sheets of aeromagnetic data occupying the study area were acquired from the Nigerian Geological Survey Agency (NGSA). Each sheet is 55 by 55 km, and the study's total covered area is roughly 257,125 sq. km. The Total Magnetic Intensity (TMI) grid occupying the study area was obtained and processed to produce the TMI map using Oasis Montaj software. The separation of residual and regional grids to create residual and regional maps of the study area came after this. The residual grid was subjected to a single block window (SBW) approach to produce eighty-five (85) equal square blocks, and the radial power spectrum algorithm was used to calculate the spectral of each block.

Estimating Curie Point Depth

Curie Point Depth (CPD) is the depth at which a ferromagnetic material loses its magnetism and the temperature at that depth is known as the Curie Temperature or Curie Point (T_c). To estimate the Curie Point (basal) Depth, Z_b, of the magnetic source, Tanaka et al., (1999) assumed that the layer of the magnetic source extends infinitely in all horizontal direction and that the depth to a magnet source's horizontal scale, and the magnetization M(x,y) is a random function of x and y. Blakely (1995) showed that the power density Spectra of the total field anomaly P;

$$P(k_x, k_y) = P_m(k_x, k_y) \times F(k_x, k_y) \text{ (Blakely,1995)} \quad 1$$

$$F(k_x, k_y) = 4\pi^2 {C_m}^2 |\theta_m|^2 |\theta_f|^2 e^{-2|k|z_t}\left[1 - e^{-|k|(z_b - z_t)}\right]^2 \text{ (Blakely, 1995)} \quad 2$$

Where P_M is the power density spectrum of the Magnetization, C_m

is proportionality constant, θ_m and θ_f are factors for the Magnetization and geomagnetic field direction respectively. Z_b and Z_t are the depths to the bottom and top of the magnetic source respectively. The equation can be simplified by noting that all terms except $|\theta_m|^2$ and $|\theta_f|^2$ are radially symmentric. Furthermore, the radial averages of θ_m and $\theta_f$are constant. If P(x,y) is completely random and uncorrelated, $P(k_x, k_y)$ Is a constant. Hence, the radial average of P is:

$$P(|k|) = Ae^{-2|k|z_t}\left[1 - e^{-|k|(z_b - z_t)}\right]^2 \quad 3$$

Where A is a constant and k is the wave number. For wavelengths less than about twice the thickness of the later Equation (3) can be written as

$$\ln P|k|^{\frac{1}{2}} = \ln B - |k|Z_t \quad 4$$

Where B is constant. The upper bound if magnetic source (Z_t) can be estimated from the slope (by fitting a straight line through the high-wave number part) radially average power spectrum $[\ln P|k|^{\frac{1}{2}}]$.

$$P|k|^{\frac{1}{2}} = Ce^{-|k|z_o}(e^{-|k|(z_t - z_o)} - e^{-|k|(z_b - z_o)} \quad 5$$

Where C is a constant, a long wavelength, equation (5) can be rewritten as

$$P|k|^{\frac{1}{2}} = Ce^{-|k|z_o}(e^{-|k|(-s)} - e^{-|k|(s)}) \approx Ce^{-|k|z_o}2|k|s \quad 6$$

Where 2s I'd the thickness of the magnetic source. From equation (3.16), it can be concluded that

$$\ln\left\{\frac{[P|k|]^{\frac{1}{2}}}{|k|}\right\} = \ln D - |k|Z_o \quad 7$$

Where D is a constant, the centroid of the magnetic source Z_o can be estimated by fitting a straight line through the lower-wave number part if the radially average frequency scale power spectrum average power. Then the Basal Depth Z_b assumed to be the CPD (Okubo et al., 1994, Kasidi and Nur, 2014;) of the magnetic source can be calculated from the equation, thus,

$$Z_b = 2Z_o - Z_t \quad 8$$

Where Z_o is the depth to centroid of the magnetic source and Z_t is the depth to the top of the magnetic anomalous body (source). At the basal depth, Z_b, ferromagnetic minerals are converted to paramagnetic minerals due to a temperature of approximately 580 °C (853 K), at that depth.

Estimating Geothermal Gradient

Geothermal gradient (GTG) is the rate the earth's temperature increases with depth, indicating heat flowing from the earth's interior to the surface.

The basic relation for conductive heat transport is the Fourier's law. Tanaka et al. (1995) showed that any given depth of a thermal Isotherm is inversely proportional to the heat flow. In a one-dimensional case under assumption that the direction of the temperature variation is vertical and the temperature gradient $\frac{dT}{dZ}$ is constant, Fourier's law takes the form

$$q = k\frac{dT}{dZ} \quad 9$$

q is the heat flux measured in units of energy, with the SI unit given as W/m^2. k is the coefficient of thermal conductivity which is a measure of how easily heat flows through a material, the SI unit for k is Wm^{-1}K^{-1} or Wm^{-1}°C^{-1}. $\frac{dT}{dZ}$ is the temperature gradient. The thermal gradient is being calculated as follows

$$\frac{dT}{dZ} = \frac{T_c - T_s}{Z_b} \quad 10$$

Where Ts is the surface temperature. An average geothermal gradient of the Earth approximately 30°Ckm^{-1} (Nemzer et al., 2009; Barbier, 2002; Kersey, 2015).

Mohammed et al. (2019) claim that temperature affects the strength and magnetic susceptibility of the crust's constituent materials. When temperatures rise above the Curie point, induced and remanent magnetization vanish, and magnetic ordering becomes loose. However, when temperatures surpass 580°C, ductile deformation starts to occur in certain materials. Then,

$$\frac{dT}{dZ} = \frac{580°C}{Z_b} \quad 11$$

Estimating Heat Flow

The heat flow (HF) values are calculated using

$$q = k\frac{dT}{dZ} \quad 12$$

Where q is the heat flow and k the coefficient of thermal conductivity. The k value differs within the study area; the variation in this value is as result of the different rocks units that are within the study area. Consequently, the thermal conductivity of rock units that are within the study area. Consequently, the thermal conductivity of rock units within each HRAM data sheets were average and used for computing the HF for each block and then for the study area. Thermal values for this study range from 1.2 Wm^{-1}°C^{-1} to 3 Wm^{-1}°C^{-1} and the average value is 2.5 Wm^{-1}°C^{-1} for the study area.

RESULTS AND DISCUSSION

The TMI data acquired was gridded to produce the total magnetic intensity (TMI) grid map as shown in Figure 2 below. The earth magnetic anomaly field is a combination of the effects of both deeper, broader sources known as regional and local sources which are consider as noise and as well as anomalies of interest otherwise residual anomalies. The difference between the observed field data (Y) and the regional field data ($\bar{Y}$) gives the residual field data. The residual and regional maps are presented in Figures 3 (a&b) below.

Science World Journal Vol. 20(No 1) 2025 https://dx.doi.org/10.4314/swj.v20i1.16
www.scienceworldjournal.org
ISSN: 1597-6343 (Online), ISSN: 2756-391X (Print)
Published by Faculty of Science, Kaduna State University

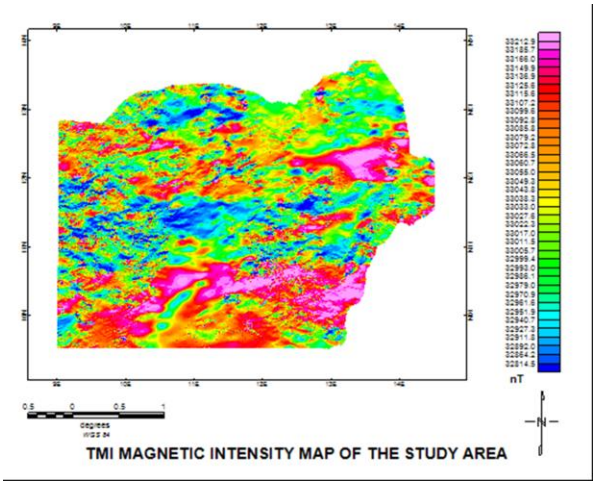

Figure 2: Total Magnetic Intensity (TMI)I Map of the Study Area

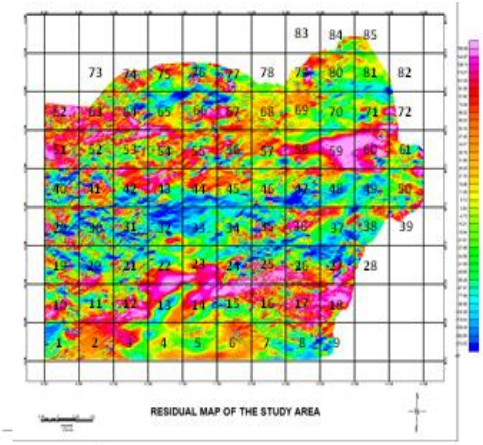

Figure 3(a): Residual Map of the Study Area

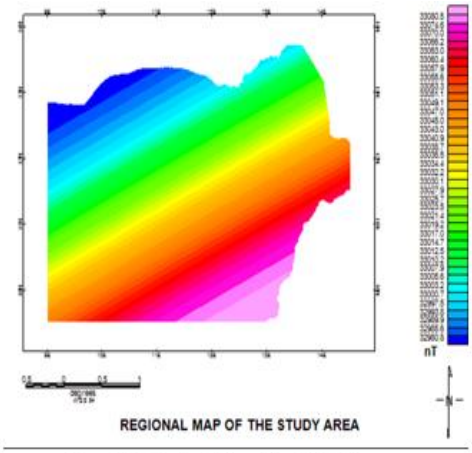

Figure 3(b): Regional Map of the Study Area

Blocks (sheets) 1 to 85 comprised the eighty-five (85) spectral blocks that made up the residual map. The power spectrum algorithm of the MAGMAP step-by-step filtering program was used for the spectral analysis. The results of the radially average power spectrum plots for blocks 1 and 2 are displayed in Figures 4 (a & b). This was achieved for all the blocks. The results were imported in excel to estimate the depth to top and depth to centroid of each block. All spectral plots obtained from the radially average power spectrum are shown in Figures 5 for only block 1 as samples, all other plots are in Appendix A (to be available on request). The estimated depth to top (Z_t) and depth to centroid (Z_o) for each block is as displayed on the spectral plot. Table 1 below shows all the results obtained for (Z_t) and (Z_o).

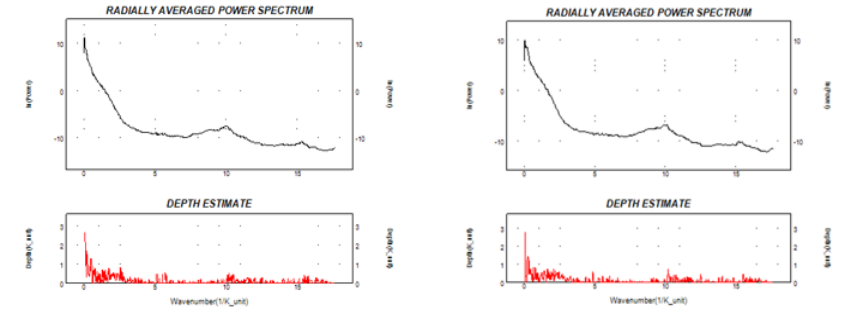

a: Block 1. **b:** Block 2.

Figure 4: The Power Radial Energy Spectrum plots.

Science World Journal Vol. 20(No 1) 2025 https://dx.doi.org/10.4314/swj.v20i1.16
www.scienceworldjournal.org
ISSN: 1597-6343 (Online), ISSN: 2756-391X (Print)
Published by Faculty of Science, Kaduna State University

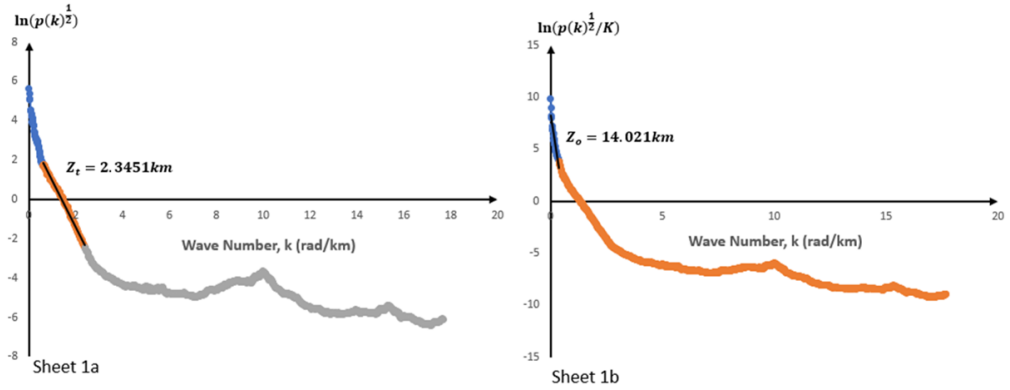

Figure 5: Spectral Plots for Block (Sheet) 1

Table 1 below shows all the results obtained for depth to top (Z_t), depth to centroid (Z_o), the longitude and latitude for each block, and the estimated CPD (Z_b). The coordinates of each block and CPD values were used to produce the CPD map (Figure 6). The values of CPD estimated range between 10.3 Km and 50.6 Km with a mean of 34.0 Km. The Geothermal Gradient (GTG) values for all the blocks were computed using their respective CPD. The GTG values as well as their respective coordinates were used to produce the GTG map (Figure 7). The estimated values range from 11.5 °CKm^{-1} to 56.4 °CKm^{-1} with a mean of 18.1 °CKm^{-1}. Table 1 above showed all the CPG, GTG and HF results obtained for all the blocks. The HF values as well as their respective coordinates were used to produce the HF map of the study area (figure 8). The estimated values range from 28.6 mWm^{-2} to 141.0 mWm^{-2} with a mean of 45.4 mWm^{-2}.

Table 1: Results of estimated Z_o, Z_t, CPD (Z_b), GTG ($\frac{dT}{dz}$) and HF (q) for all the blocks

BLOCK	LONG (°)	LAT (°)	z_o (Km)	z_t (Km)	z_b (Km)	$\frac{dT}{dz}$ ($^{\circ}C/Km$)	q mWm^{-2}
1	9.25	9.75	14.021	2.3451	25.6969	22.57082	56.42704
2	9.75	9.75	12.03	2.2002	21.8598	26.53272	66.33181
3	10.25	9.75	16.809	1.9363	31.6817	18.3071	45.76775
4	10.75	9.75	6.0483	1.815	10.2816	56.41145	141.0286
5	11.25	9.75	20.97	1.8124	40.1276	14.45389	36.13473
6	11.75	9.75	16.038	2.2281	29.8479	19.43185	48.57963
7	12.25	9.75	17.689	2.4157	32.9623	17.59586	43.98965
8	12.75	9.75	22.023	2.9277	41.1183	14.10564	35.2641
9	13.25	9.75	18.799	3.2039	34.3941	16.86336	42.15839
10	9.25	10.25	16.078	2.2943	29.8617	19.42287	48.55718
11	9.75	10.25	18.334	2.2669	34.4011	16.85993	42.14981
12	10.25	10.25	14.36	2.38	26.34	22.01974	55.04935
13	10.75	10.25	13.606	1.7522	25.4598	22.78101	56.95253
14	11.25	10.25	22.936	2.8706	43.0014	13.48793	33.71983
15	11.75	10.25	20.563	2.2763	38.8497	14.92933	37.32333
16	12.25	10.25	10.887	2.3884	19.3856	29.91912	74.79779
17	12.75	10.25	14.826	2.5789	27.0731	21.42348	53.5587
18	13.25	10.25	11.358	2.1816	20.5344	28.24529	70.61321
19	9.25	10.75	9.4039	2.31	16.4978	35.1562	87.89051
20	9.75	10.75	20.703	2.3924	39.0136	14.86661	37.16653
21	10.25	10.75	15.315	2.3988	28.2312	20.54465	51.36161
22	10.75	10.75	26.457	4.9554	47.9586	12.09376	30.23441
23	11.25	10.75	18.813	1.3967	36.2293	16.00914	40.02285
24	11.75	10.75	21.8	2.4176	41.1824	14.08369	35.20922
25	12.25	10.75	15.031	2.3698	27.6922	20.94453	52.36131

26	12.75	10.75	15.865	2.4451	29.2849	19.80543	49.51357
27	13.25	10.75	15.643	2.4993	28.7867	20.14819	50.37048
28	13.75	10.75	19.797	4.1185	35.4755	16.34931	40.87328
29	9.25	11.25	21.103	2.4483	39.7577	14.58837	36.47092
30	9.75	11.25	17.048	2.1799	31.9161	18.17265	45.43162
31	10.25	11.25	13.659	2.1724	25.1456	23.06567	57.66416
32	10.75	11.25	19.216	3.093	35.339	16.41246	41.03116
33	11.25	11.25	24.055	7.127	40.983	14.15221	35.38052
34	11.75	11.25	23.308	2.8854	43.7306	13.26302	33.15756
35	12.25	11.25	15.235	2.4108	28.0592	20.67058	51.67646
36	12.75	11.25	25.701	2.672	48.73	11.90232	29.7558
37	13.25	11.25	21.502	3.1851	39.8189	14.56595	36.41487
38	13.75	11.25	14.064	2.6737	25.4543	22.78593	56.96484
39	14.25	11.25	18.18	3.3885	32.9715	17.59095	43.97737
40	9.25	11.75	16.007	2.4764	29.5376	19.63599	49.08997
41	9.75	11.75	18.157	2.7176	33.5964	17.26375	43.15939
42	10.25	11.75	15.794	2.6944	28.8936	20.07365	50.18412
43	10.75	11.75	15.925	3.3862	28.4638	20.37676	50.9419
44	11.25	11.75	18.638	3.9396	33.3364	17.3984	43.496
45	11.75	11.75	16.193	4.5466	27.8394	20.83378	52.08446
46	12.25	11.75	15.284	3.4976	27.0704	21.42562	53.56404
47	12.75	11.75	19.23	3.7528	34.7072	16.71123	41.77807
48	13.25	11.75	20.861	4.0271	37.6949	15.3867	38.46674
49	13.75	11.75	19.36	3.6054	35.1146	16.51735	41.29337
50	14.25	11.75	21.774	4.7098	38.8382	14.93375	37.33438
51	9.25	12.25	16.963	3.0714	30.8546	18.79785	46.99461
52	9.75	12.25	17.553	3.056	32.05	18.09672	45.24181
53	10.25	12.25	23.787	3.4056	44.1684	13.13156	32.8289
54	10.75	12.25	15.791	3.7749	27.8071	20.85798	52.14496
55	11.25	12.25	20.869	4.0622	37.6758	15.3945	38.48624
56	11.75	12.25	19.613	3.6153	35.6107	16.28724	40.7181
57	12.25	12.25	22.939	3.6148	42.2632	13.72352	34.30881
58	12.75	12.25	25.282	4.873	45.691	12.69397	31.73491
59	13.25	12.25	18.547	2.9606	34.1334	16.99215	42.48039
60	13.75	12.25	23.03	7.4753	38.5847	15.03186	37.57966
61	14.25	12.25	25.907	9.0715	42.7425	13.56963	33.92408
62	9.25	12.75	20.596	3.259	37.933	15.29012	38.22529
63	9.75	12.75	14.785	2.9999	26.5701	21.82905	54.57262
64	10.25	12.75	17.472	3.1646	31.7794	18.25082	45.62704
65	10.75	12.75	20.346	3.3102	37.3818	15.51557	38.78893
66	11.25	12.75	15.959	3.4499	28.4681	20.37368	50.9342
67	11.75	12.75	18.629	4.4456	32.8124	17.67624	44.19061
68	12.25	12.75	17.307	6.7098	27.9042	20.7854	51.9635
69	12.75	12.75	20.85	6.9952	34.7048	16.71239	41.78096
70	13.25	12.75	22.366	7.5982	37.1338	15.61919	39.04798
71	13.75	12.75	24.204	5.0065	43.4015	13.36359	33.40898
72	14.25	12.75	26.482	9.553	43.411	13.36067	33.40167
73	9.75	13.25	18.036	2.7657	33.3063	17.41412	43.53531

Science World Journal Vol. 20(No 1) 2025 https://dx.doi.org/10.4314/swj.v20i1.16
www.scienceworldjournal.org
ISSN: 1597-6343 (Online), ISSN: 2756-391X (Print)
Published by Faculty of Science, Kaduna State University

74	10.25	13.25	18.403	2.6394	34.1666	16.97564	42.43911
75	10.75	13.25	19.071	3.9723	34.1697	16.9741	42.43526
76	11.25	13.25	20.328	4.0702	36.5858	15.85315	39.63286
77	11.75	13.25	16.126	4.7204	27.5316	21.0667	52.66675
78	12.25	13.25	26.542	5.7009	47.3831	12.24065	30.60163
79	12.75	13.25	23.597	6.781	40.413	14.35182	35.87954
80	13.25	13.25	21.295	8.164	34.426	16.84773	42.11933
81	13.75	13.25	27.565	4.5153	50.6147	11.45912	28.6478
82	14.25	13.25	25.327	9.739	40.915	14.17573	35.43933
83	12.75	13.75	20.378	6.4542	34.3018	16.90873	42.27183
84	13.25	13.75	23.439	7.5096	39.3684	14.73263	36.83157
85	13.75	13.75	21.047	7.3098	34.7842	16.67424	41.68559
Min			6.0483	1.3967	10.2816	11.45912	28.6478
Max			27.565	9.739	50.6147	56.41145	141.0286
Mean			18.90504	3.795072	34.015	18.14257	45.35641
Std Dev			4.171957	1.924367	7.366651	5.844095	14.61024

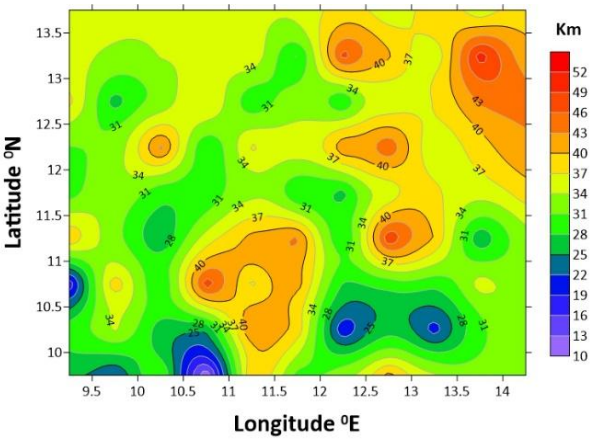

Figure 6: Curie Point Depth Contour Map of the Study Area (Contour interval of 3 Km)

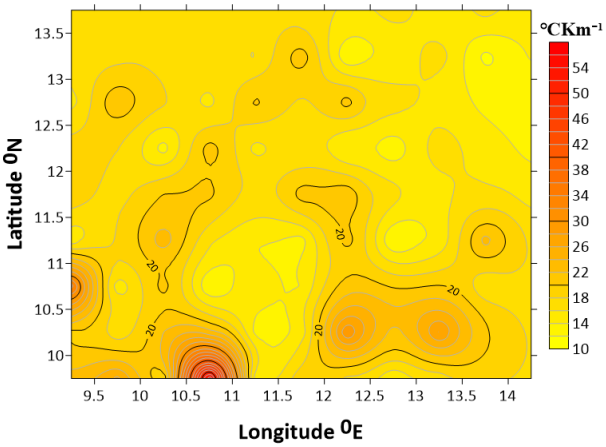

Figure 7: GTG Contour Map of the Study Area (Contour interval of 3 °C/km)

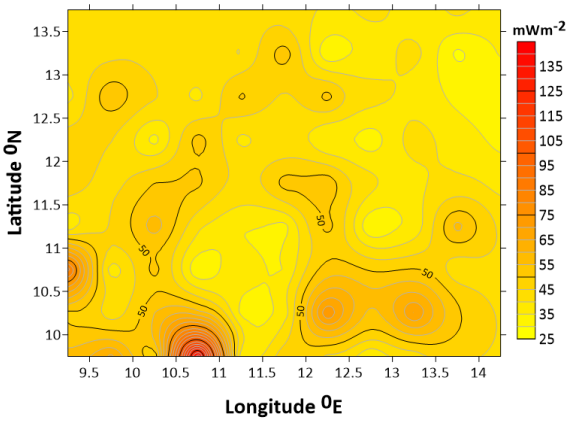

Figure 8: HF Contour Map of the Study Area (Contour interval of 6 $mW\,\mathrm{m}^{-2}$)

The research area's total magnetic intensity map (TMI) (Figure 2) demonstrates that the magnetic intensity of the study area is divided into regions of high and low magnetic signatures. The map's pink coloration indicates a high magnetic signature, whereas the blue coloration indicates a low magnetic signature. The TMI map of the research area clearly shows the high magnetic signature region in the southern and some northeastern parts, indicating the high magnetic signature trends southeast. Differential magnetic susceptibilities, lithology, depth variations, and strike angles can all contribute to variations in magnetic signatures. The research area's northwestern section exhibits a less prominent high magnetic signature than the northern and western sections, which are both characterized by a low magnetic signature.

In the regional map (Figure 3b), it was observed that the trend pattern is NE-SW which is in conformity with most tectonic structures. The values of the regional field of the aeromagnetic data were increasing from NW to SE section.

The research area's residual magnetic intensity map (Figure 3a) displays the magnetic intensity values, which vary from -210.0 to

168.6 nT. The research area's southern, northwest, and northeast regions are where the highest magnetic anomaly signatures are primarily seen. Nonetheless, sporadic traces are also seen, primarily in the study area's northern regions. Throughout the middle region of the research area, low magnetic anomaly signs are seen trending eastward. Low magnetic anomalies are connected to the sedimentary region, but high magnetic anomalies could be the consequence of basement intrusion into the strata (Mohammed et al., 2019).

The research region's Curie point depth contour map (Figure 6) shows that the southern portion of the area is covered in low depths, while the northeastern and certain areas of the central portion have high CPD. Tanaka et al. (1999) reported that different geological contexts typically result in significant variations in the CPDs, and compiled CPD results from multiple researchers worldwide and concluded that CPDs shallower than 10 km are found in volcanic, tectonic, and associated geodynamic environments, while CPDs between 15 and 25 km are caused by island arcs and ridges, and deeper than 25 km are found in plateaus and trenches.

The GTG contour map (Figure 6) shows that high GTG above 30 $°\mathrm{C/km}$ is observed in the southern part, with very high values in the southwest region of the study area. The computed HF values range between 28.65 and 141.03 $\mathrm{mWm^{-2}}$, with an average of 45.36 $\mathrm{mWm^{-2}}$. The research area's HF exhibits a SW trending and increasing from the central portion towards the southwest. The contour maps of the GTG and HF indicate that the GTG and the HF are closely connected, and most regions with high HF also have significant geothermal gradients. The heat flow anomalies are found around the Kerri formation, tertiary to recent volcanic, and metamorphic (Bima sandstone and Yolde formation) areas. According to Mohammed et al. (2019), all current literature states that CPD and HF greatly depend on geological conditions, whereas HF is the primary observable parameter in geothermal exploration, and generally high HF values correspond to volcanic and metamorphic regions since the two units have high heat conductivities. Additionally, tectonically active regions have a significant impact on heat flow (Tanaka et al., 1999). Geothermal energy does also occur in areas where basement rocks that have relatively normal heat flow are covered by a thick blanket of thermally insulated sediments (Mohammed et al., 2019).

In thermally normal continental regions, the average HF is about 60 $\mathrm{mWm^{-2}}$, values between 80 and 100 $\mathrm{mWm^{-2}}$ are good geothermal sources, while values greater than 100 $\mathrm{mWm^{-2}}$ are an indication of anomalous geothermal conditions (Nwankwo and Sunday, 2017). In view of this, areas with high HF values make the study area favorable for geothermal potential.

According to Nwankwo and Sunday (2017), the average HF in continental regions that are thermally typical is approximately 60 $\mathrm{mWm^{-2}}$; values in the range of 80 to 100 $\mathrm{mWm^{-2}}$indicate a good geothermal source; values over 100 $\mathrm{mWm^{-2}}$ indicate abnormal geothermal conditions (Mohammed et al., 2019). For this reason, the research region has favorable geothermal potential in locations with high HF values.

Conclusion

The research area's estimated CPD results show that the CPD varies inversely with HF, indicating a decrease in HF in the study area as the CPD increases. With an average of 34.02 km, the estimated Curie point depth values vary between 10.28 and 50.61 km. This indicates that Curie depths are a good indirect indicator of the research area's thermal structure. With an average of 18.14 °C/km, the research area's computed geothermal gradient values range from 11.46 to 56.42 °C/km. With an average of 45.36 $\mathrm{mWm^{-2}}$, the HF values, obtained from the research area's geothermal gradient values, range from 28.65 to 141.03 $\mathrm{mWm^{-2}}$. The outcome is favorable as it can be applied to investigate geothermal energy in the research region as a potential alternative energy source, especially in regions with low values of CPD and high HF values.

Acknowledgment

The authors acknowledge the support from the grants TETF/DR&D/UNI/ZARIA/IBR/2024/BATCH 8/06.

REFERENCES

Abraham, M.E. (2011). *Interpretation of Aeromagnetic Data for Geothermal Energy of Ikogosi warm Spring Area of Ekiti State, Southwestern Nigeria.* M.Sc. Thesis Dept. of Physics ABU Zaria. Unpublished M.Sc. thesis.

Barbier, E. (2002). *Geothermal energy technology and current status: An overview*. Renewable and Sustainable Energy Reviews 2002: 3-65. Print.

Blakely, R.J. (1995). Potential Theory in Gravity and Magnetic Applications. *Cambridge Univ. Press*, pp. 307-308.

Bowyer, D., Bratkovich, D.S, Frank, M. and Fernholz, K. (2011). Geothermal 101: *The Basics and Applications of Geothermal Energy*. Adam Zoet. 2011 Dovetail partners, Inc.

Cole, C.A. (2014). "*Review of Geothermal Heating and Cooling of Buildings*" 2nd Climatic Change Technology Conference.

Dada, S.S. and Suh, C.E. (2006). Finding Economic Uranium Deposits and the Nigerian Energy mix: Implications for National Development. In: Abaa SI, Baba S (eds.), Proc. first Petr. Tech. Dev. Fund (PTDF) Workshop, University of Maiduguri, pp. 34 – 48.

Ewa, K. and Kryrowska, S. (2010). Geothermal exploration in Nigeria. Proceedings World Geothermal Congress. Zaria, Nigeria, (3); 1 – 59.

Fridleifsson, I.B., Bertani, R., Huenges, E., Lund, J.W., Ragnarsson, A. and Rybach, L. (2008). The possible role and contribution of geothermal energy to the mitigation of climate change. *Luebeck, Germany, pp. 59–80.*

Funtua, I.I., Okujeni, C.D. and Elegba, S.B. (1999). Preliminary Note on the Geology and Genetic Model of Uranium Mineralization in Northeastern *Nigeria. J. Min. Geol.* 35(2):125 – 136.

GEA, (2012). Geothermal basic Questions and Answers. http://geotehrmal.org/what.html.pp8.

GRC (2017). Advancing Geothermal Development through Education Outreach and Dissemination of Research. http://geothermal.org/whathtml.

Hulen, J.B. and Wright, P.M. (2001). Geothermal Energy: Sustainable Energy for the Benefit of Humanity and the Environment. Energy & Geoscience Institute, University of Utah.

Islam, M.R. and Baba, S. (1990). The mineral potential of the northern part of Mandara hills, Nigeria. Berg-und huttenmannische monatshefe (BHM) 135(4):95 –98.

Jalo, M.E. (2015). Geology and petrography of the rocks around Gulani Area, Northeastern Nigeria. Journal of Geology

and Mining Research,7(5), pp. 41-57.

Kasidi, S. and Nur, A. (2014). Estimation of Curie Point Depth, Heat Flow and Geothermal Gradient Inferred from Aeromagnetic data over Jalingo and Environs North-Eastern Nigeria. *International Journal of Science and Emerging Technologies*, 6(6).

Kersey, W. (2015). Geothermal Energy and its Application in the Modern World 6.15.2015. www.indiana.edu/seira/papers/2015/kerseypdf.

Lawal, T. O., Nwankwo, L.I., IWA, A.A., Sunday, J.A. and Orosun, M.M. (2018). Geothermal Energy Potential of the Chad Basin, North-Eastern *Nigeria. J. Appl. Sci. Environ. Manage.* Vol. 22 (11) 1817–1824

Mohammed A., Adewumi T., Kazeem S. A., Abdulwaheed R., Adetona A. A. and Usman A. (2019). Assessment of Geothermal Potentials in some Parts of Upper Benue Trough Northeast Nigeria Using Aeromagnetic Data. *Journal of Geoscience, Engineering, Environment, and Technology*. Vol 04 No 01.

Nemzer, M.L., Carter, A.K. and Nemzer, K.P. (2004). Geothermal energy facts: Geothermal Education Office, online at: http://geothermal.marin.org/pwrheat.html.

Nemzer, M.L., Carter, A.K. and Nemzer, K.P. (2009). Geothermal Energy. Microsoft Encarta 2009 (DVD). Redmond, W.A.: Microsoft Corporation, 2008.

Nwankwo, L.I. and, Sunday, A.J. (2017). Regional Estimation of Curie Point Depths and Succeeding Geothermal Parameters from Recently Acquired High- Resolution Aeromagnetic data of the Entire Bida Basin, North-Central Nigeria. *Geotherm. Energy Sci.* 1, 9.

Obande, G.E., Lawal, K.M. and Ahmed, L.A. (2014). Spectral Analysis of Aeromagnetic Data for Geothermal Investigation of Wikki Warm Spring, North-East Nigeria. *Geothermics*, 50, 85-90.

Okubo, Y. and Matsunaga, T. (1994). Curie Point Depth in Northeast Japan and its Correlation with regional thermal structure and seismicity. *Journal of geophysical Research: Solid Earth*, 99(B11), 22363-22371.

Oyedepo, S.O. (2012). Energy and sustainable development in Nigeria: The way forward. *Energy, Sustainability and Society*. 2:15.

Rabeh, T., Abdallatif, T., Mekkawi, M., Khalil, A. and El-emam, A. (2008). Magnetic data interpretation and depth estimation constraints: a correlative study on magnetometer and gradiometer data. *NRIAG J. Geophys* (Special Issue): 185 209.

Ravat, D; Pignatelli, A; Nicolosi, I; Chiappini, M (2007). A study of spectral method of estimating the depth to the bottom of magnetic sources from near-surface magnetic anomaly data. *Geophys. J. Int.* 169: 421 – 434.

Renewable Energy World (2019). Geothermal Energy. https://www.renewableenergyworld.com /geotehrmalenergy/tech/geoelectricity.html Copyright 1999-2019 RenewableEnergy World.com - All rights reserved.

Sunday, E.S. (2015). Renewable: Exploring Geothermal for Electrification. Daily Trust Monday October 26. http://www.dailytrust.com.ng.

Sunday, O., Elijah, A. A., Samuel, B. O. and Caroline, O. D. (2022). Investigation of geothermal potential of the Dahomey basin, Nigeria, through analysis of geomagnetic and geo-resistivity dataset, *NRIAG Journal of Astronomy and Geophysics,* 11:1, 373-386, DOI: 10.1080/20909977.2022.2141022.

Tanaka, A., Okubo, T. and Matsubayashi, O. (1999). Curie Point Depth based on Spectrum Analysis of the Magnetic Anomaly Data in east and Southeast Asia. *Tectonophysics*, 306(3), 461-470.

Turcotte, D. L. and Schubert, G. (2002). Geodynamics (2 ed.), Cambridge, England, UK: Cambridge University Press, pp. 136–137, ISBN 978-0-521-66624-4

World Energy Council (2014). http://www.worldenergy.org/data/trilemma index/country/Nigeria /2014/.